

Topology Optimization of High Power Electronic Devices

Ronald H.W. Hoppe, Svetozara Petrova, and Volker Schulz

Abstract. Modern high power electronic devices such as converter modules used as electric drives for high power electromotors are characterized by extremely high switched currents and very fast switching times. The avoidance of significant losses in the power transmission due to parasitic inductivities requires a subtle layout of the devices. Using the electric conductivity as a design parameter and electromagnetic potentials associated with the eddy currents equations as the state variables, the design issue gives rise to a topology optimization with both equality and inequality constraints where the design objective is to distribute the material in such a way that the electromagnetic energy dissipation is minimized. Based on appropriate finite element approximations of the eddy currents equations, for the numerical solution of the discretized optimization problem we suggest a primal-dual Newton interior-point method with a hierarchy of two merit functions and a watchdog strategy for convergence monitoring.

1. Introduction

The optimal design of mechanical structures described by continuum mechanical models is by now a well established discipline both with regard to mathematical theory, numerical simulation, and engineering applications. It includes shape and topology optimization as well as the design of composites by homogenization approaches (cf., e.g., the textbooks [5, 17, 28, 31], and the references therein). On the other hand, the use of modern discretization and numerical solution techniques such as multigrid and domain decomposition methods in an optimization framework, in particular their appropriate combination with advanced optimization approaches, is still in its infancy (cf., e.g., [7, 10, 18, 22, 23, 25], and [30]).

As far as the optimal design and layout of electronic devices and systems are concerned, a lot of work has been done in electric circuitry with emphasis on the application of discrete optimization techniques (cf., e.g., [1] and [11]), but considerably less work has been devoted to the optimization of devices and systems whose operational behavior is strongly dictated by Maxwell's equations.

Key words and phrases. topology optimization, high power electronic devices, eddy currents, edge elements, primal-dual interior-point methods, watchdog strategy.

In this contribution, we consider an optimal design problem arising in high power electronics, namely the layout of converter modules that are used as electric drives for high power electromotors. The objective is to minimize power losses due to parasitic inductivities by an optimal distribution of the material. From a mathematical point of view, this leads to a topology optimization problem where the design variable, the electric conductivity, and the state variables, the generated electromagnetic fields resp. the associated potentials, are subject to equality and inequality constraints. In particular, the scalar electric potential and the magnetic vector potential are required to satisfy the potential formulation of the eddy currents equations given by the quasistationary limit of Maxwell's equations. As far as the numerical solution is concerned, we use finite element methods based on curl-conforming edge elements for the magnetic vector potential and nonconforming P1 elements (Crouzeix-Raviart elements) for the scalar electric potential. The discretized optimization problem is then solved by a primal-dual Newton interior-point method featuring logarithmic barrier functions to take care of the inequality constraints and a simultaneous sequential quadratic programming approach for the resulting equality constrained minimization subproblems. The convergence to a local minimizer is monitored by a hierarchy of two merit functions used within an appropriate watchdog strategy.

2. The Topology Optimization Problem

A typical example for a high power electric device is a converter module designed to convert dc into ac or vice versa and to be used in electric drives for high power electromotors. As shown in Figure 1, a converter module consists of modern semiconductor devices such as IGBTs (Insulated Gate Bipolar Transistors) or GTOs (Gate Turn-Off Thyristors) interconnected and linked with the high power voltage source and load by copper made bus bars. The IGBTs and GTOs that can be viewed as valves for the electric currents admit switching times of less than 100 nanoseconds and switched currents up to five kiloamperes. Figure 2 shows the typical 3D geometry of a bus bar with several ports where the semiconductor devices can be attached.

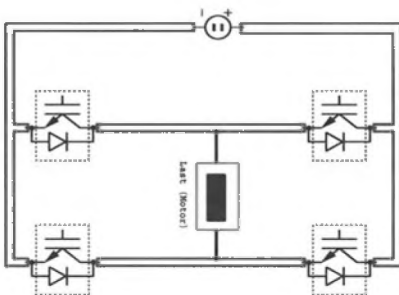


Fig. 1: Converter Module



Fig. 2: Geometry of a bus bar

The problem that occurs is that due the fast switching times and steep current ramps, eddy currents build up inside the bus bars causing parasitic inductivities that lead to a considerable loss in the power transmission (cf. [12]). Therefore, the primary goal is to design the bus bars in such a way that the energy dissipation is minimized. It is known that the topology of the bus bars plays a prominent role in so far as it has a significant impact on the distribution and size of the generated eddy currents. Consequently, the task is to distribute the material in an optimal way. From a mathematical point of view, the problem will be stated as a topology optimization problem with constraints on the state and design variables.

The eddy currents are described by the quasistationary limit of Maxwell's equations

$$\frac{\partial \mathbf{B}}{\partial t} + \operatorname{curl} \mathbf{E} = \mathbf{0} \quad , \quad \operatorname{div} \mathbf{B} = 0 \quad , \quad \operatorname{curl} \mathbf{H} = \mathbf{J} \quad , \quad (1)$$

$$\mathbf{B} = \mu \mathbf{H} \quad , \quad \mathbf{J} = \sigma \mathbf{E} \quad , \quad (2)$$

where \mathbf{E} , \mathbf{H} denote the electric and the magnetic field, \mathbf{B} is the magnetic induction, \mathbf{J} stands for the current density, and the material parameters μ, σ refer to the magnetic permeability and the electric conductivity, respectively. Following [6], we resort to a potential formulation by introducing a scalar electric potential φ and a magnetic vector potential \mathbf{A} according to

$$\mathbf{E} = -\operatorname{grad} \varphi - \frac{\partial \mathbf{A}}{\partial t} \quad , \quad \mathbf{B} = \operatorname{curl} \mathbf{A} \quad . \quad (3)$$

Considering a module $\Omega = \cup_{\nu=1}^N \Omega_\nu$ with N bars Ω_ν , $1 \leq \nu \leq N$, each bar containing N_ν ports $\Gamma_{\nu\alpha}$, $1 \leq \alpha \leq N_\nu$, and denoting by $I_{\nu\alpha}$ the flux at the port $\Gamma_{\nu\alpha}$, we are thus led to the following coupled system of PDEs

$$\operatorname{div} (\sigma \operatorname{grad} \varphi) = 0 \quad \text{in} \quad \Omega \quad , \quad (4)$$

$$\sigma \mathbf{n} \cdot \operatorname{grad} \varphi = \begin{cases} -I_{\nu\alpha}(t) & \text{on } \Gamma_{\nu\alpha} \\ 0 & \text{elsewhere} \end{cases} \quad (5)$$

$$\sigma \frac{\partial \mathbf{A}}{\partial t} + \operatorname{curl} \mu^{-1} \operatorname{curl} \mathbf{A} = \begin{cases} -\sigma \operatorname{grad} \varphi & \text{in } \Omega \\ 0 & \text{in } \mathbf{R}^3 \setminus \bar{\Omega} \end{cases} \quad (6)$$

with appropriate initial and boundary conditions. The energy dissipation on $[0, T]$ is then given by

$$L = \int_0^T \int_{\Omega} \mathbf{J} \cdot \mathbf{E} \, dx \, dt \quad . \quad (7)$$

Taking (1),(2) and (3) into account, we may view L as a functional depending on the conductivity σ which will serve as the design parameter and on the potentials φ, \mathbf{A} which are chosen as the state variables. Prescribing the total amount of material in terms of the conductivity and allowing σ to vary between a maximum value σ_{\max} (conductivity of copper) and a minimum value $0 < \sigma_{\min} := \varepsilon \ll 1$ which

is chosen small but positive in order to keep the ellipticity of the problem, we are faced with the topology optimization problem

$$\inf_{\sigma, \varphi, \mathbf{A}} L(\sigma, \varphi, \mathbf{A}) \quad (8)$$

subject to the equality constraints

$$\varphi \text{ and } \mathbf{A} \text{ satisfy the state equations (4),(5),(6),} \quad (9)$$

$$\int_{\Omega} \sigma \, dx = C \quad (10)$$

and the inequality constraints

$$\sigma_{\min} \leq \sigma \leq \sigma_{\max} . \quad (11)$$

In order to enforce the extreme values σ_{\max} and σ_{\min} , we use the SIMP-approach (Simple Isotropic Material with Penalization) known from structural mechanics. In the present context, it means that we "replace" the conductivity σ by

$$\eta(\sigma) = \left(\frac{\sigma - \sigma_{\min} + \varepsilon}{\sigma_{\max} - \sigma_{\min}} \right)^q \quad (12)$$

with an appropriately chosen penalty parameter $q \geq 1$.

3. The Primal-dual Newton Interior-point Method

In this section, we will present a primal-dual Newton interior-point method for the numerical solution of the discretized optimization problem. Realizing the exterior domain by an artificial exterior boundary and using simplicial triangulations $\mathcal{T}_h^{(I)}, \mathcal{T}_h^{(E)}$ of the interior and exterior domain, the discretization is performed by applying the implicit Euler scheme in time and curl-conforming edge elements of lowest order [26] in space to (6) whereas nonconforming Crouzeix-Raviart elements are used for (4),(5). The conductivity is approximated by elementwise constants, i.e., $\vec{\sigma} = (\sigma_1, \dots, \sigma_{m_h})^T$, $m_h = \text{card } \mathcal{T}_h^{(I)}$. The discretized state variables are denoted by $\vec{\varphi} = (\varphi_1, \dots, \varphi_{n_h})^T$ and $\vec{A} = (A_1, \dots, A_{p_h})^T$ where n_h, p_h are the dimensions of the associated nonconforming resp. edge element spaces. For notational convenience, we comprise them to a vector $\vec{u} = (\vec{\varphi}, \vec{A})$ and refer to

$$A(\vec{\sigma}) \vec{u} = \vec{b} \quad (13)$$

as the discretized state equations with $A(\vec{\sigma})$ denoting the matrix of the associated system of equations. The constraints (10) and (11) take the form

$$g(\vec{\sigma}) := \sum_{i=1}^{m_h} |K_i| \sigma_i = C, \quad (14)$$

$$\sigma_{\min} \vec{e} \leq \vec{\sigma} \leq \sigma_{\max} \vec{e}, \quad (15)$$

where $K_i \in \mathcal{T}_h^{(I)}$, $1 \leq i \leq m_h$, and $\vec{e} := (1, \dots, 1)^T$.

Denoting the discretized objective functional by $L_h(\vec{u}, \vec{\sigma})$, the discrete optimization problem reads as follows:

$$\min_{\vec{u}, \vec{\sigma}} L_h(\vec{u}, \vec{\sigma}) \tag{16}$$

subject to the constraints (13),(14), and (15).

We note that the discretization can be performed within a multilevel and/or domain decomposition framework by means of multigrid iterative solvers based on edge element discretizations of the implicitly in time discretized equation for the magnetic vector potential (6) and nonconforming P1 approximations of the equation for the scalar electric potential (5) (cf., e.g., [2, 24]) or domain decomposition methods on nonmatching grids with respect to a nonoverlapping geometrically conforming partition of the computational domain dictated by the geometry of the bus bars (cf., e.g., [4, 8, 19, 20, 29]). For adaptive grid refinement/coarsening relying on efficient and reliable a posteriori error estimators we refer to [2, 3].

In contrast to traditional design strategies where the optimization loop consists of the numerical solution of the field equations for the current design followed by a Newton-type procedure for the computation of the increments for the design parameters, we will use an integrated approach by means of a primal-dual Newton interior-point method where the convergence is monitored by a hierarchy of merit functions combined with an appropriate watchdog strategy. Such techniques have been recently developed and tested for nonlinear programming problems (cf., e.g., [13, 14, 16]). Typically, the inequality constraints are taken care of by classical logarithmic barrier functions with a barrier parameter resulting in a parametrized family of minimization subproblems which is then solved by a simultaneous sequential quadratic programming technique.

The first step in the primal-dual interior-point approach is to introduce the logarithmic barrier functions

$$B(\vec{u}, \vec{\sigma}, p) := L_h(\vec{u}, \vec{\sigma}) - p [\log(\vec{\sigma} - \sigma_{\min} \vec{e}) + \log(\sigma_{\max} \vec{e} - \vec{\sigma})], \tag{17}$$

where $p > 0$ is a suitably chosen barrier parameter. We consider the family of minimization subproblems

$$\min_{\vec{u}, \vec{\sigma}} B(\vec{u}, \vec{\sigma}, p) \tag{18}$$

subject to the equality constraints

$$A(\vec{\sigma})\vec{u} = \vec{b} \quad , \quad g(\vec{\sigma}) = C \tag{19}$$

For an isolated local minimum $(\vec{u}^*, \vec{\sigma}^*)$ of (16) it can be shown that for a null sequence $(p_n)_{\mathbb{N}}$ of sufficiently small barrier parameters the minimization problems (18) have solutions $(\vec{u}_n, \vec{\sigma}_n)$ converging to $(\vec{u}^*, \vec{\sigma}^*)$.

The second step is to invoke a simultaneous SQP approach for the solution of (18). To be more specific, the equality constraints (19) are coupled by Lagrangian multipliers leading to the saddle point problem

$$\min_{\vec{u}, \vec{\sigma}} \max_{\vec{\lambda}, \eta} \mathcal{L}^{(p)}(\vec{u}, \vec{\sigma}, \vec{\lambda}, \eta) \tag{20}$$

for the Lagrangian

$$\mathcal{L}^{(p)}(\vec{u}, \vec{\sigma}, \vec{\lambda}, \eta) := B(\vec{u}, \vec{\sigma}, p) + \vec{\lambda}^T (A(\vec{\sigma})\vec{u} - \vec{b}) + \eta(g(\vec{\sigma}) - C). \quad (21)$$

The Karush-Kuhn-Tucker conditions are given by

$$\mathcal{F}^{(p)}(\vec{u}, \vec{\sigma}, \vec{\lambda}, \eta) = 0, \quad (22)$$

where

$$\begin{aligned} \mathcal{F}_1^{(p)} &= \nabla_{\vec{u}} \mathcal{L}^{(p)} = \nabla_{\vec{u}} L + A(\vec{\sigma})^T \vec{\lambda}, \\ \mathcal{F}_2^{(p)} &= \nabla_{\vec{\sigma}} \mathcal{L}^{(p)} = \partial_{\vec{\sigma}} (\vec{\lambda}^T A(\vec{\sigma})\vec{u}) + \eta \nabla_{\vec{\sigma}} g(\vec{\sigma}) - p D_1^{-1} \vec{e} + p D_2^{-1} \vec{e}, \\ \mathcal{F}_3^{(p)} &= \nabla_{\vec{\lambda}} \mathcal{L}^{(p)} = A(\vec{\sigma})\vec{u} - \vec{b}, \\ \mathcal{F}_4^{(p)} &= \nabla_{\eta} \mathcal{L}^{(p)} = g(\vec{\sigma}) - C, \end{aligned}$$

and $D_1 := \text{diag}(\sigma_i - \sigma_{\min})$ and $D_2 := \text{diag}(\sigma_{\max} - \sigma_i)$.

Since for $p \rightarrow 0$ the expressions $p D_1^{-1} \vec{e}$ and $p D_2^{-1} \vec{e}$ approximate the complementarity conditions associated with (16), it is standard to introduce $\vec{z} := p D_1^{-1} \vec{e}$ and $\vec{w} := p D_2^{-1} \vec{e}$ as some kind of approximate complementarity. Then, Newton's method is applied to three sets of equations

- primal feasibility $(\vec{u}, \vec{\sigma})$,
- dual feasibility $(\vec{\lambda}, \eta)$,
- perturbed complementarity (\vec{z}, \vec{w})

resulting in the linear algebraic system

$$\begin{pmatrix} 0 & \mathcal{L}_{\vec{u}\vec{\sigma}} & \mathcal{L}_{\vec{u}\vec{\lambda}} & 0 & 0 & 0 \\ \mathcal{L}_{\vec{\sigma}\vec{u}} & \mathcal{L}_{\vec{\sigma}\vec{\sigma}} & \mathcal{L}_{\vec{\sigma}\vec{\lambda}} & \mathcal{L}_{\vec{\sigma}\eta} & -I & I \\ \mathcal{L}_{\vec{\lambda}\vec{u}} & \mathcal{L}_{\vec{\lambda}\vec{\sigma}} & 0 & 0 & 0 & 0 \\ 0 & \mathcal{L}_{\eta\vec{\sigma}} & 0 & 0 & 0 & 0 \\ 0 & Z & 0 & 0 & D_1 & 0 \\ 0 & -W & 0 & 0 & 0 & D_2 \end{pmatrix} \begin{pmatrix} \Delta \vec{u} \\ \Delta \vec{\sigma} \\ \Delta \vec{\lambda} \\ \Delta \eta \\ \Delta \vec{z} \\ \Delta \vec{w} \end{pmatrix} = - \begin{pmatrix} \nabla_{\vec{u}} \mathcal{L} \\ \nabla_{\vec{\sigma}} \mathcal{L} \\ \nabla_{\vec{\lambda}} \mathcal{L} \\ \nabla_{\eta} \mathcal{L} \\ \nabla_{\vec{z}} \mathcal{L} \\ \nabla_{\vec{w}} \mathcal{L} \end{pmatrix}. \quad (23)$$

Note that the coefficient matrix is usually referred to as the primal-dual Hessian. Obviously, it is not symmetric but can be easily symmetrized, since the matrices Z and W are diagonal (cf., e.g., [15]). We do not adapt this approach here, but instead perform a block elimination of the increments $\Delta \vec{z}$ and $\Delta \vec{w}$ yielding the condensed system

$$\begin{pmatrix} 0 & \mathcal{L}_{\vec{u}\vec{\sigma}} & \mathcal{L}_{\vec{u}\vec{\lambda}} & 0 \\ \mathcal{L}_{\vec{\sigma}\vec{u}} & \tilde{\mathcal{L}}_{\vec{\sigma}\vec{\sigma}} & \mathcal{L}_{\vec{\sigma}\vec{\lambda}} & \mathcal{L}_{\vec{\sigma}\eta} \\ \mathcal{L}_{\vec{\lambda}\vec{u}} & \mathcal{L}_{\vec{\lambda}\vec{\sigma}} & 0 & 0 \\ 0 & \mathcal{L}_{\eta\vec{\sigma}} & 0 & 0 \end{pmatrix} \begin{pmatrix} \Delta \vec{u} \\ \Delta \vec{\sigma} \\ \Delta \vec{\lambda} \\ \Delta \eta \end{pmatrix} = - \begin{pmatrix} \nabla_{\vec{u}} \mathcal{L} \\ \tilde{\nabla}_{\vec{\sigma}} \mathcal{L} \\ \nabla_{\vec{\lambda}} \mathcal{L} \\ \nabla_{\eta} \mathcal{L} \end{pmatrix}, \quad (24)$$

where

$$\tilde{\mathcal{L}}_{\vec{\sigma}\vec{\sigma}} := \mathcal{L}_{\vec{\sigma}\vec{\sigma}} + D_1^{-1} Z + D_2^{-1} W, \quad \tilde{\nabla}_{\vec{\sigma}} \mathcal{L} := \nabla_{\vec{\sigma}} \mathcal{L} - D_1^{-1} \nabla_{\vec{z}} \mathcal{L} + D_2^{-1} \nabla_{\vec{w}} \mathcal{L}.$$

Following [25], we consider a null space decomposition of the condensed primal-dual Hessian, i.e., we interchange the second and third rows and columns and partition the resulting matrix according to

$$\mathcal{K} = \begin{pmatrix} \mathcal{A} & \mathcal{B}^T \\ \mathcal{B} & \mathcal{D} \end{pmatrix} = \left(\begin{array}{cc|cc} 0 & \mathcal{L}_{\vec{u}\vec{\lambda}} & \mathcal{L}_{\vec{u}\vec{\sigma}} & 0 \\ \mathcal{L}_{\vec{\lambda}\vec{u}} & 0 & \mathcal{L}_{\vec{\lambda}\vec{\sigma}} & 0 \\ \hline \mathcal{L}_{\vec{\sigma}\vec{u}} & \mathcal{L}_{\vec{\sigma}\vec{\lambda}} & \tilde{\mathcal{L}}_{\vec{\sigma}\vec{\sigma}} & \mathcal{L}_{\vec{\sigma}\eta} \\ 0 & 0 & \mathcal{L}_{\eta\vec{\sigma}} & 0 \end{array} \right). \quad (25)$$

We remark that the first diagonal block

$$\mathcal{A} = \begin{pmatrix} 0 & \mathcal{L}_{\vec{u}\vec{\lambda}} \\ \mathcal{L}_{\vec{\lambda}\vec{u}} & 0 \end{pmatrix}$$

is indefinite, but nonsingular with $\mathcal{L}_{\vec{\lambda}\vec{u}}$ being the stiffness matrix $A(\vec{\sigma})$ associated with the discretized potential equations.

We choose $\tilde{A}(\vec{\sigma})$ as an appropriate approximation of $A(\vec{\sigma})$ realized, for instance, by an SSOR iteration. Then, for

$$\mathcal{K}^R = \begin{pmatrix} I & -\tilde{A}^{-1}\mathcal{B}^T \\ 0 & I \end{pmatrix} = \left(\begin{array}{cc|cc} I & 0 & -\tilde{A}^{-1}(\vec{\sigma})\mathcal{L}_{\vec{\lambda}\vec{\sigma}} & 0 \\ 0 & I & -\tilde{A}^{-1}(\vec{\sigma})\mathcal{L}_{\vec{u}\vec{\sigma}} & 0 \\ \hline 0 & 0 & I & 0 \\ 0 & 0 & 0 & I \end{array} \right) \quad (26)$$

and taking advantage of the regular splitting

$$\mathcal{K}\mathcal{K}^R = \underbrace{\begin{pmatrix} 0 & A(\vec{\sigma}) & | & 0 & 0 \\ A(\vec{\sigma}) & 0 & | & 0 & 0 \\ \hline \mathcal{L}_{\vec{\sigma}\vec{u}} & \mathcal{L}_{\vec{\sigma}\vec{\lambda}} & | & \tilde{S} & \mathcal{L}_{\vec{\sigma}\eta} \\ 0 & 0 & | & \mathcal{L}_{\eta\vec{\sigma}} & 0 \end{pmatrix}}_{=: \mathcal{M}_1} - \underbrace{\begin{pmatrix} 0 & 0 & | & \mathcal{L}_{\vec{u}\vec{\sigma}} - A(\vec{\sigma})\tilde{A}^{-1}(\vec{\sigma})\mathcal{L}_{\vec{u}\vec{\sigma}} & 0 \\ 0 & 0 & | & \mathcal{L}_{\vec{\lambda}\vec{\sigma}} - A(\vec{\sigma})\tilde{A}^{-1}(\vec{\sigma})\mathcal{L}_{\vec{\lambda}\vec{\sigma}} & 0 \\ \hline 0 & 0 & | & 0 & 0 \\ 0 & 0 & | & 0 & 0 \end{pmatrix}}_{=: \mathcal{M}_2}$$

where

$$\tilde{S} := \tilde{\mathcal{L}}_{\vec{\sigma}\vec{\sigma}} - \mathcal{L}_{\vec{\sigma}\vec{u}}\tilde{A}^{-1}(\vec{\sigma})\mathcal{L}_{\vec{\lambda}\vec{\sigma}} - \mathcal{L}_{\vec{\sigma}\vec{\lambda}}\tilde{A}^{-1}(\vec{\sigma})\mathcal{L}_{\vec{u}\vec{\sigma}},$$

we perform the transforming iterations

$$\Delta\Psi^{\nu+1} = \Delta\Psi^\nu + \mathcal{K}^R \mathcal{M}_1^{-1} (d - \mathcal{K} \Delta\Psi^\nu), \quad (27)$$

where $\Delta\Psi := (\Delta\vec{u}, \Delta\vec{\lambda}, \Delta\vec{\sigma}, \Delta\eta)^T$. The new iterate $\Psi^{(\text{new})} := (\vec{u}^{(\text{new})}, \vec{\lambda}^{(\text{new})}, \vec{\sigma}^{(\text{new})}, \eta^{(\text{new})})^T$ is then obtained by a line search in the direction $\Delta\Psi$:

$$\Psi_i^{(\text{new})} = \Psi_i^{(\text{old})} + s_i (\Delta\Psi)_i, \quad 1 \leq i \leq 4. \quad (28)$$

A standard convergence monitor in nonlinear programming is to choose the Euclidean norm $\|\mathcal{F}^{(p)}(\vec{u}, \vec{\sigma}, \vec{\lambda}, \eta)\|$ of the residual with respect to the KKT-conditions (22) as a merit function. However, in the situation under consideration this is an

inappropriate tool, since it does not allow to tell the difference between a local minimizer and a stationary nonminimizing point. Indeed, the computations reveal that using the residual as a merit function one often gets stuck with a saddle point. A better approach is to rely on a hierarchy of two merit functions (cf., e.g., [16, 27]). In particular, the primary merit function is chosen as a modified augmented Lagrangian incorporating the logarithmic barrier functions according to

$$M_1(\vec{x}, \vec{y}, p, p_A) := L_h(\vec{x}) - p \sum_{i=1}^2 \log d_i(\vec{x}) + \vec{y}^T \vec{c}(\vec{x}) + \frac{1}{2} p_A \vec{c}(\vec{x})^T \vec{c}(\vec{x}) \quad (29)$$

where $\vec{x} := (\vec{u}, \vec{\sigma})^T$, $\vec{y} := (\vec{\lambda}, \eta)^T$, $\vec{c}(\vec{x}) := (c_1(\vec{x}), c_2(\vec{x}))^T$, and

$$\begin{aligned} c_1(\vec{x}) &:= A(\vec{\sigma})\vec{u} - \vec{b} \quad , \quad c_2(\vec{x}) := g(\vec{\sigma}) - C \quad , \\ d_1(\vec{x}) &:= \vec{\sigma} - \sigma_{\min} \vec{e} \quad , \quad d_2(\vec{x}) := \sigma_{\max} \vec{e} - \vec{\sigma} \quad . \end{aligned}$$

Note that p_A is a positive penalty parameter. For p_A sufficiently large it is always possible to realize a decrease in M_1 .

The residual with respect to the KKT-conditions is chosen as the secondary merit function

$$M_2(\vec{x}, \vec{y}) := \|\mathcal{F}_p(\vec{u}, \vec{\sigma}, \vec{\lambda}, \eta)\| \quad . \quad (30)$$

In practice, the hierarchy of merit functions is used by means of the following strategy: If the steplengths s_i , $1 \leq i \leq 4$, lead to a decrease in M_1 , they are accepted. If M_1 does not decrease, M_2 is checked and the steplengths are accepted in case it has decreased. However, if there is no reduction of M_1 after at most N_{wd} iterations, the penalty parameter p_A is chosen sufficiently large in order to guarantee a decrease in M_1 . Note that in our computations $N_{\text{wd}} = 4$ turned out to be a suitable choice.

4. Numerical Results

The simulation results obtained by the application of the primal-dual Newton interior-point method can be displayed by a grey-scale representing the range of the computed material distribution from dark ($\sigma = \sigma_{\max}$) to light ($\sigma = \sigma_{\min}$). Figures 3 and 4 show such a scale for a 2D computation where the bar contains 2 ports (Fig. 3) resp. 6 ports (Fig. 4) with a current inflow at the upper port(s) and an equal amount of current outflow at the lower port, and the design objective is to minimize the electric energy dissipation. In particular, Figure 3 displays the influence of the penalty parameter q in (12) on the material distribution whereas Figure 4 reflects the impact of the granularity of the triangulation. Table 1 contains the convergence history of the optimization algorithm where N_c stands for the number of ports, N_x resp. N_y are the numbers of nodal points in x- resp. y-direction, "iter" is the number of required iterations with $\|\mathcal{F}_p^k\| \leq 10^{-6} \|\mathcal{F}_p^0\|$ as stopping criterion (\mathcal{F}_p^k denotes the k-th residual), "p" is the last value of the barrier parameter, " M_1 " and $\|\mathcal{F}_p\|_2$ are the final values of the primary and secondary

merit functions, and $\|v\|_2$ is the ℓ_2 -norm related to the compatibility conditions at the last iteration. In all experiments the watchdog never "barked", i.e., we achieved a reduction of the primary merit function within the prescribed maximal number of watchdog iterations. For more details concerning the performance of the primal-dual Newton interior-point method and the watchdog strategy we refer to [22]. We remark that the numerical results are usually postprocessed in order to obtain a strict material/no material distribution (cf., e.g., [5]).

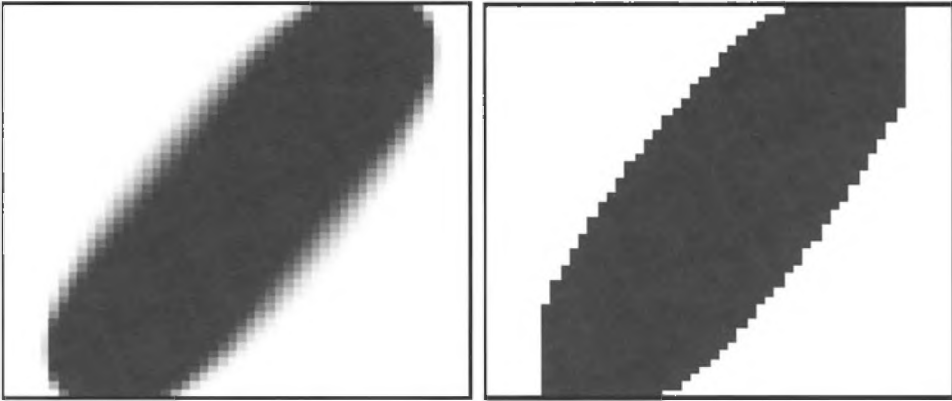


Fig. 3: Material distribution (2 contacts, $q=1$ (left) and $q=2$ (right))

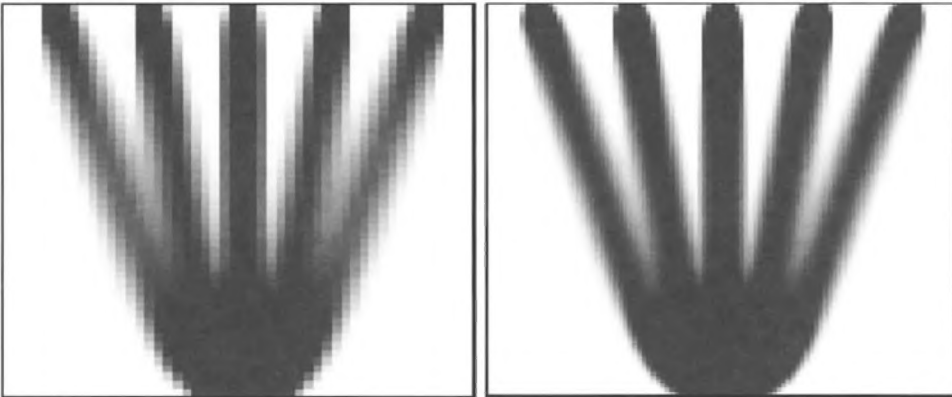


Fig. 4: Material distribution (6 contacts)
 50×50 mesh (left) and 100×100 mesh (right)

For an individual optimized 3D bus bar with prescribed fluxes through the ports, Figure 4 displays the computed magnetic induction between two ports illustrating the effect of the holes.

Finally, we note that the primal-dual techniques described in the previous section lead to considerable savings in computational time compared to traditional approaches and allow to determine local minima representing improved designs by a margin between 10% and 20% depending on the specific operating conditions.

N_c	N_x	N_y	q	iter	p	M_1	$\ \mathcal{F}_p\ _2$	$\ \mathbf{v}\ _2$
2	25	25	1	17	4.92e-17	4.69	9.64e-4	e-9
2	25	25	2	19	4.29e-18	4.83	2.85e-5	e-9
2	50	50	1	19	1.28e-18	5.10	2.99e-4	e-10
2	50	50	2	90	1.18e-9	5.23	5.70e-3	e-6
3	50	50	1	30	6.44e-19	3.78	2.40e-4	e-11
3	50	50	2	75	1.07e-6	4.33	9.67e-3	e-4
3	100	100	1	84	3.68e-17	4.05	3.35e-4	e-9
3	100	100	2	24	1.78e-7	4.20	9.69e-3	e-5
6	50	50	1	20	9.85e-17	85.99	1.27e-3	e-9
6	50	50	2	45	9.64e-7	97.46	1.61e-2	e-4
6	100	100	1	24	3.46e-17	84.30	7.62e-4	e-9
6	100	100	2	43	4.18e-7	89.12	1.64e-2	e-5

TABLE 1. Convergence history

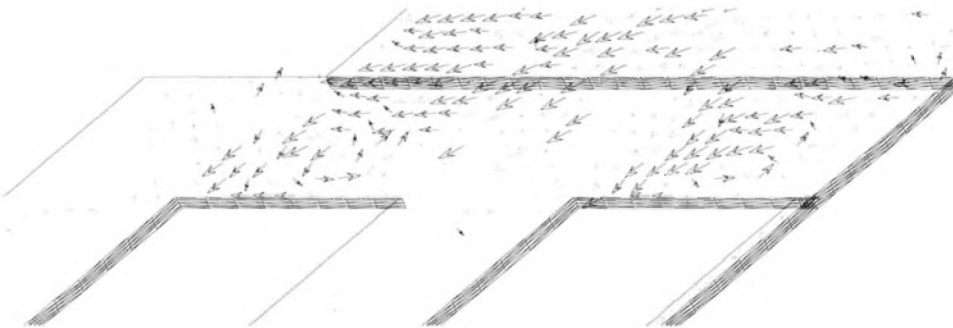


Fig. 5: Magnetic induction in converter module (zoom)

Acknowledgments. The work of the first author has been supported by a grant from the Federal Ministry for Education and Research (BMBF) under Grant No. 03HO7AU1-8. The second author is indebted to the Alexander-von-Humboldt Foundation for an AvH-Fellowship. The first and the second author are also grateful for grants from the German National Science Foundation (DFG; Grant No. HO877/4-1 and HO877/5-1).

References

- [1] Chr. Albrecht, B. Korte, J. Schietke, and J. Vygen, “Cycle time and slack optimization for VLSI-chips”, Rep. No. 99881, Forschungsinstitut für Diskrete Mathematik, Bonn, (1999).
- [2] R. Beck, P. Deuffhard, R. Hiptmair, R.H.W. Hoppe, and B. Wohlmuth, “Adaptive multilevel methods for edge element discretizations of Maxwell’s equations”, *Surveys of Math. in Industry*, Vol. 8, pp. 271–312, (1999).
- [3] R. Beck, R. Hiptmair, R.H.W. Hoppe, and B. Wohlmuth, “Residual based a posteriori error estimators for eddy current computation”, *M²AN Mathematical Modelling and Numerical Analysis* 34, 159–182, (2000).
- [4] F. Ben Belgacem, A. Buffa, and Y. Maday, “The mortar finite element method for 3D Maxwell equations: First results”, Report 99023, Laboratoire d’Analyse Numérique, Université Pierre et Marie Curie, Paris, (1999).
- [5] M.P. Bendsøe, “Optimization of Structural Topology, Shape, and Material”, Springer, Berlin-Heidelberg-New York, (1995).
- [6] O. Biro and K. Preis, “Various FEM formulations for the calculation of transient 3D eddy currents in nonlinear media”, *IEEE Trans. Magn.* 31, 1307–1312 (1995).
- [7] G. Biros and O. Ghattas, “Parallel preconditioners for KKT systems arising in optimal control of viscous incompressible flows”. to appear in: Proc. Parallel CFD ’99, Williamsburg, Virginia, May 23–26, 1999, North Holland, Amsterdam, London, New York, (2000).
- [8] P. Böhm, R.H.W. Hoppe, G. Mazurkevitch, S. Petrova, G. Wachutka, and E. Wolfgang, “Optimal design of high power electronic devices by topology optimization”, to appear in: *Mathematik – Schlüsseltechnologie für die Zukunft. Verbundprojekte zwischen Mathematik und Industrie*, Springer, Berlin-Heidelberg-New York, (2001).
- [9] Th. Borrvall and J. Petersson, “Topology optimization using regularized intermediate density control”, Techn. Rep. LiTH-IKP-R-1086, Department of Mechanical Engineering, University of Linköping, (2000).
- [10] A. Borzi and K. Kunisch, “A multigrid method for optimal control of time-dependent reaction diffusion processes”. to appear in: Proc. Workshop “Fast Solution of Discretized Optimization Problems”, Weierstrass Institute Berlin, May 08–12, 2000 (K.-H. Hoffmann, R.H.W. Hoppe, V. Schulz; eds.), Birkhäuser, Basel, (2000).
- [11] K. Doll, F.M. Johannes, and K.J. Antreich, “Iterative placement improvement by network flow methods”, *IEEE Trans. Comp.-Aided Design Integr. Circuits and Systems CAD-13*, 1190–1200, (1994).
- [12] St. Dürndorfer, V. Gradinaru, R.H.W. Hoppe, E.-R. König, G. Schrag, and G. Wachutka, “Numerical simulation of microstructured semiconductor devices, transducers, and systems”, In: *High Performance Scientific and Engineering Computing. Proc. ”Int. FORTWIHR-Symposium”*, Munich, March 1998 (Bungartz, H., Durst, F., and Zenger, Chr.; eds.), pp. 309–323, *Lecture Notes in Computational Science and Engineering*, Vol. 8, Springer, Berlin-Heidelberg-New York, (1999).
- [13] A.S. El-Bakry, R.A. Tapia, T. Tsuchiya, and Y. Zhang, “On the formulation of the Newton interior-point method for nonlinear programming”, *Journal of Optimization Theory and Applications* 89, 507–541 (1996).

- [14] A. Forsgen and Ph. Gill, “Primal-dual interior methods for nonconvex nonlinear programming”, *SIAM J. Optimization* **8**, 1132–1152 (1998).
- [15] A. Forsgen, Ph. Gill, and J.R. Shinnerl, “Stability of symmetric ill-conditioned systems arising in interior methods for constrained optimization”, *SIAM J. Matrix Anal. Appl.* **17**, 187–211, (1996).
- [16] D.M. Gay, M.L. Overton, and M.H. Wright, “A primal-dual interior method for nonconvex nonlinear programming”, Techn. Rep. 97-4-08, Computing Science Research Center, Bell Laboratories, Murray Hill, New Jersey, 1997.
- [17] J. Haslinger and P. Neittaanmäki, “Finite Element Approximation for Optimal Shape Design: Theory and Applications”, J. Wiley & Sons, Chichester, 1988.
- [18] M. Heinkenschloss, “Time-domain decomposition iterative methods for the solution of parabolic linear-quadratic optimal control problems”, Techn. Rep., Department of Comput. and Appl. Math., Rice University, Houston, (2000).
- [19] R.H.W. Hoppe, “Mortar edge elements in \mathbf{R}^3 ”, *East-West J. Numer. Anal.*, Vol. **7**, 159–173, (1999).
- [20] R.H.W. Hoppe, “Adaptive mortar edge elements in the computation of eddy currents”, In: Proc. Conf. “Analysis and Approximation of Boundary Value Problems”, Jyväskylä, Finland, October 1998 (P. Neittaanmäki et al.; eds.), pp. 83–96, Dept. Math. Inf. Techn., No. A 2/2000, Jyväskylä, 2000.
- [21] R.H.W. Hoppe, Y. Iliash, and G. Mazurkevitch, “Domain decomposition methods in the design of high power electronic devices”, In: Proc. Conf. on Multifield Problems, Stuttgart, October 1999 (M. Sändig and W. Wendland, eds.), pp. 169–182, Springer, Berlin-Heidelberg-New York, (2000).
- [22] R.H.W. Hoppe, S. Petrova, and V. Schulz, “A primal-dual Newton-type interior-point method for topology optimization”, Preprint, Institute of Mathematics, University of Augsburg, (2000).
- [23] R.H.W. Hoppe, S. Petrova, and V. Schulz, “Topology optimization of conductive media described by Maxwell’s equations”, to appear in Proc. 2nd Conf. Numer. Anal. Appl., Rouse, Bulgaria, Lect. Notes in Comp. Sci., Springer,(2001).
- [24] R.H.W. Hoppe and B. I. Wohlmuth, “Adaptive multilevel iterative techniques for nonconforming finite element discretizations”, *East-West J. Numer. Math.* **3**, 179–197, (1995).
- [25] B. Maar and V. Schulz, “Interior point multigrid methods for topology optimization”, *Structural Optimization* **19**, 214–224, (2000).
- [26] J.-C. Nédélec, “Mixed finite elements in \mathbf{R}^3 ”, *Numer. Math.* **35**, 315–341, (1980).
- [27] Z. Parada and R.A. Tapia, “Computational experience with a modified augmented Lagrangian merit function in a primal-dual interior-point method”, Techn. Rep., Department of Comput. and Appl. Math., Rice University, Houston, (1995).
- [28] O. Pironneau, “Optimal Shape Design for Elliptic Systems”, Springer, Berlin-Heidelberg-New York, (1984).
- [29] F. Rapetti, Y. Maday, and F. Bouillaud, “The mortar edge element method in three dimensions: application to magnetostatics”, Preprint, ASCI-UPR 9029 CNRS, Paris Sud University, Orsay, (2000).

- [30] V. Schulz, “Mehrgittermethoden für Optimierungsprobleme bei PDE”, Habilitationsschrift, Universität Heidelberg, (2000).
- [31] J. Sokolowski and J.P. Zolesio, “Introduction to Shape Optimization”, Springer, Berlin-Heidelberg-New York, (1992).

Institute of Mathematics

University of Augsburg

D-86159 Augsburg, Germany

E-mail address: hoppe@math.uni-augsburg.de

E-mail address: petrova@math.uni-augsburg.de

Weierstrass Institute for Applied Analysis and Stochastics

D-10117 Berlin, Germany

E-mail address: vschulz@na-net.ornl.gov